Inhibition of FAAH confers increased stem cell migration via PPARα

Yvonne Wollank,*,† Robert Ramer,* Igor Ivanov,* Achim Salamon,† Kirsten Peters,† and Burkhard Hinz[1,*]

Institute of Toxicology and Pharmacology* and Department of Cell Biology,† Rostock University Medical Center, D-18057 Rostock, Germany

Abstract **Regenerative activity in tissues of mesenchymal origin depends on the migratory potential of mesenchymal stem cells (MSCs). The present study focused on inhibitors of the enzyme fatty acid amide hydrolase (FAAH), which catalyzes the degradation of endocannabinoids (anandamide, 2-arachidonoylglycerol) and endocannabinoid-like substances (*N*-oleoylethanolamine, *N*-palmitoylethanolamine). Boyden chamber assays, the FAAH inhibitors, URB597 and arachidonoyl serotonin (AA-5HT), were found to increase the migration of human adipose-derived MSCs. LC-MS analyses revealed increased levels of all four aforementioned FAAH substrates in MSCs incubated with either FAAH inhibitor. Following addition to MSCs, all FAAH substrates mimicked the promigratory action of FAAH inhibitors. Promigratory effects of FAAH inhibitors and substrates were causally linked to activation of p42/44 MAPKs, as well as to cytosol-to-nucleus translocation of the transcription factor, PPARα. Whereas PPARα activation by FAAH inhibitors and substrates became reversed upon inhibition of p42/44 MAPK activation, a blockade of PPARα left p42/44 MAPK phosphorylation unaltered. Collectively, these data demonstrate FAAH inhibitors and substrates to cause p42/44 MAPK phosphorylation, which subsequently activates PPARα to confer increased migration of MSCs. This novel pathway may be involved in regenerative effects of endocannabinoids whose degradation could be a target of pharmacological intervention by FAAH inhibitors.**—Wollank, Y., R. Ramer, I. Ivanov, A. Salamon, K. Peters, and B. Hinz. **Inhibition of FAAH confers increased stem cell migration via PPARα. *J. Lipid Res.* 2015.** 56: **1947–1960.**

Supplementary key words fatty acid amide hydrolase inhibitors • endocannabinoids • peroxisome proliferator-activated receptor α • mesenchymal stem cells

Since the discovery of cannabinoid receptors and their endogenously synthesized ligands in the 1990s, an avalanche of reports has suggested that the endocannabinoid system contributes to a broad array of physiological functions [for review see (1)]. As a consequence, components of this system, as well as pharmacological strategies to block endocannabinoid degradation, have been elucidated in past years [for review see (2)].

An integral component of the endocannabinoid system is the enzyme, fatty acid amide hydrolase (FAAH), a serine hydrolase first identified as the principal catabolic enzyme of the endocannabinoid, anandamide [*N*-arachidonoylethanolamine (AEA)] (3). The second major endocannnabinoid, 2-arachidonoylglycerol (2-AG), can be hydrolyzed by multiple enzymes, including FAAH and monoacylglycerol lipase (MAGL), with about 85% of brain 2-AG hydrolase activity ascribed to MAGL (4). Likewise, FAAH is the catabolic enzyme for the endocannabinoid-like substances, *N*-oleoylethanolamine (OEA) and *N*-palmitoylethanolamine (PEA) (5). In contrast to AEA and 2-AG, both endocannabinoid-like substances do not bind to the cannabinoid receptors, CB_1 and CB_2, but share an activation of the nonselective cation channel transient receptor potential vanilloid 1 (TRPV1) (6–9) and the transcription factor PPARα (10–16) with endocannabinoids. In line with the latter notion, various biological effects of FAAH inhibitors have been associated with activation of PPARα (17–21).

Several components of the endocannabinoid system, including CB_1, CB_2, TRPV1, and cannabinoid receptor ligands, have been reported as effectors of tissue healing

Abbreviations: AA-5HT, *N*-arachidonoyl serotonin; AEA, *N*-arachidonoylethanolamine; 2-AG, 2-arachidonoylglycerol; AM-251, *N*-(piperidin-1-yl)-5-(4-iodophenyl)-1-(2,4-dichlorophenyl)-4-methyl-1H-pyrazole-3-carboxamine; AM-630, {6-Iodo-2-methyl-1-[2-(4-morpholinyl)ethyl]-1H-indol-3-yl}(4-methoxyphenyl)methanone; CB_1, cannabinoid receptor 1; CB_2, cannabinoid receptor 2; FAAH, fatty acid amide hydrolase; GW6471, *N*-[(2S)-2-[[(1Z)-1-methyl-3-oxo-3-[4-(trifluoromethyl)phenyl]-1-propen-1-yl]amino]-3-[4-[2-(5-methyl-2-phenyl-4-oxazolyl)ethoxy]phenyl]propyl]-propanamide; MAGL, monoacylglycerol lipase; MSC, mesenchymal stem cell; OEA, *N*-oleoylethanolamine; PD98059, 2-(2-amino-3-methoxyphenyl)-4H-1-benzopyran-4-one; PEA, *N*-palmitoylethanolamine; SB203580, 4-[4-(4-fluorophenyl)-2-(4-methylsulfinylphenyl)-1*H*-imidazol-5-yl]pyridine; PPARα, peroxisome proliferator-activated receptor α; TRPV1, transient receptor potential vanilloid 1; URB597, [3-(3-carbamoylphenyl)phenyl] *N*-cyclohexylcarbamate; WST-1, 4-[3-(4-Iodophenyl)-2-(4-nitrophenyl)-2H-5-tetrazolio]-1.6-benzene disulfonate; WY-14643, 4-chloro-6-(2,3-xylidino)-2-pyrimidinylthioacetic acid (pirinixic acid).

[1] To whom correspondence should be addressed.
e-mail: burkhard.hinz@med.uni-rostock.de

This study was supported by the FORUN program of the Rostock University Medical Center.

Manuscript received 24 June 2015 and in revised form 30 July 2015.

Published, JLR Papers in Press, August 11, 2015
DOI 10.1194/jlr.M061473

(22–25). As a consequence of these findings, cannabinoids have gained interest as potential options for the treatment of osteodegenerative disorders such as osteoporosis (24, 26–28) or neurodegenerative diseases such as Parkinson's disease (29). Among a variety of cellular features, previous investigations proved cannabinoids to increase tissue healing properties via induction of cellular migration at different sites such as blood vessels (30), corneal tissue (31), and colonic tissue (32). In this context, a recent study from our group found the nonpsychoactive phytocannabinoid, cannabidiol, to enhance the migratory potential of human mesenchymal stem cells (MSCs) (33). It is noteworthy that the pluripotent MSCs contribute to healing processes of injured tissues such as myocardium (34, 35), injured spots of the eye (36), and bone tissue (37, 38). Thus endocannabinoids and endocannabinoid-like substances, as well as enzymes that degrade these substances, are discussed as an endogenous system that regulates the differentiation of neural tissue (39–41), modulates embryogenesis (42), and coordinates remodeling of bone tissue (43).

Regarding the molecular mechanism underlying the promigratory effect of cannabinoids on cells of mesenchymal origin, CB_2 receptor activation has been shown to increase the migration of murine osteoblast-like cells (44). Moreover, activation of p42/44 MAPK, an essential intracellular trigger of migratory behavior of stem cells (45, 46), has recently been shown to confer the promigratory effect of cannabidiol on MSCs (33). However, the impact of the endocannabinoids, AEA and 2-AG, or the endocannabinoid-like substances, OEA and PEA, on the migratory action of MSCs is largely unknown.

The present study therefore investigates the impact of [3-(3-carbamoylphenyl)phenyl] *N*-cyclohexylcarbamate (URB597), an irreversible carbamate-based FAAH inhibitor (47–49), and *N*-arachidonoyl serotonin (AA-5HT), an endogenous molecule with FAAH inhibitory activity (50), as well as of the FAAH substrates, AEA, 2-AG, OEA, and PEA, on the migration of human MSCs and the mechanism underlying a potential response. Here we present evidence for a promigratory action of these substances involving initial phosphorylation of p42/44 MAPK and subsequent activation of PPARα.

MATERIALS AND METHODS

Materials

The 2-AG, AA-5HT, *N*-(piperidin-1-yl)-5-(4-iodophenyl)-1-(2,4-dichlorophenyl)-4-methyl-1H-pyrazole-3-carboxamine (AM-251), {6-iodo-2-methyl-1-[2-(4-morpholinyl)ethyl]-1H-indol-3-yl}(4-methoxyphenyl)methanone (AM-630), *N*-[(2S)-2-[[(1Z)-1-methyl-3-oxo-3-[4-(trifluoromethyl)phenyl]-1-propen-1-yl]amino]-3-[4-[2-(5-methyl-2-phenyl-4-oxazolyl)ethoxy]phenyl]propyl]-propanamide (GW6471), OEA, PEA, URB597, and 4-chloro-6-(2,3-xylidino)-2-pyrimidinylthioacetic acid (WY-14643) were obtained from Biomol GmbH (Hamburg, Germany). AEA and 4-[4-(4-fluorophenyl)-2-(4-methylsulfinylphenyl)-1*H*-imidazol-5-yl]pyridine (SB203580) were purchased from Enzo Life Sciences GmbH (Lörrach, Germany). The 2-(2-amino-3-methoxyphenyl)-4H-1-benzopyran-4-one (PD98059) was obtained from InvivoGen (Toulouse, France). Bisbenzimide, DMSO, EDTA, glycerol, glycine, H_2O_2, HEPES, NaCl, SDS, and Tris were obtained from AppliChem GmbH (Darmstadt, Germany). DMEM (high glucose, GlutaMAX™), penicillin/streptomycin, and trypsin/EDTA were obtained from Life Technologies GmbH (Darmstadt, Germany). FCS and PBS were bought from PAN Biotech (Aidenbach, Germany). The 2-propanol and collagenase NB4 standard grade were obtained from Serva (Heidelberg, Germany). Aprotinine, BSA, capsazepine, HCl, leupeptine, luminal, ortho-vanadate, para-couramic acid, PMSF, and Triton® X-100 were from Sigma (Taufkirchen, Germany). Milk powder was obtained from Bio-Rad Laboratories GmbH (Munich, Germany). Acrylamide (Rothiphorese® Gel 30) was obtained from Carl Roth GmbH (Karlsruhe, Germany).

Cell culture

Cultivation of primary human MSCs was performed as described recently (33). For isolation of human MSCs, subcutaneous adipose samples were acquired by liposuction. The donors had been informed about the use of cells from their tissue for scientific purposes and had given informed consent. Adipose tissue was digested in collagenase NB4 standard grade solution (6 mg/ml) with gentle agitation for 30 min at 37°C. Afterwards, the digested adipose tissue was filtered through a 100 μm nylon mesh [BD Falcon™ cell strainer (BD Biosciences, Heidelberg, Germany)], washed in 10 ml PBS with 10% (v/v) FCS, and allowed to sediment. The liquid fraction was removed and filtered through a 40 μm nylon mesh [BD Falcon™ cell strainer (BD Biosciences)]. Both fractions were centrifuged at 400 *g* for 10 min. The supernatant in both fractions was removed and the pellets were combined, resuspended in PBS containing 10% (v/v) FCS, and centrifuged at 400 *g* for 5 min. All centrifugation steps were performed at room temperature. Cells were subsequently cultured in DMEM containing 10% (v/v) FCS, 100 U/ml penicillin, and 100 μg/ml streptomycin for 24 h. From these primary cultures, MSCs were isolated via their characteristic expression of CD34 surface antigen, using the Dynabeads® CD34 positive isolation kit (Life Technologies GmbH) according to the manufacturer's instructions.

All experiments were conducted with cells from passage 4. MSCs were seeded at a density of 2×10^4 cells per cm^2, i.e., 6,800 cells per well of a 96-well plate (0.34 cm^2), 38,000 cells per well of a 24-well plate (1.9 cm^2), 192,000 cells per well of a 6-well plate (9.6 cm^2), and 1.16×10^6 cells per Petri dish (58 cm^2). The only exception was migration assays (see Migration assay) with 1×10^5 cells seeded per insert of a 24-well format Boyden chamber.

All incubations were performed in serum-free DMEM. Test substances were dissolved in ethanol or DMSO and diluted with PBS to yield final concentrations of 0.1% (v/v) ethanol (for AEA, OEA, and PEA) or 0.1% (v/v) DMSO (for AA-5HT, 2-AG, AM-251, AM-630, capsazepine, GW6471, PD98059, SB203580, and URB597), if not otherwise specified. WY-14643 was dissolved in DMSO and diluted with PBS to yield a final concentration of 0.5% (v/v) DMSO. PBS containing the respective concentration of ethanol and/or DMSO was used as vehicle control.

Migration assay

The effect of test substances on the transmigration of MSCs was determined using a modified Boyden chamber assay according to the manufacturer's instructions (BD Biosciences, Becton Dickinson GmbH, Heidelberg, Germany) as described recently (33). In this assay, cellular motility is monitored by migration through transwell inserts with pores (8 μm pore size) toward a chemoattractant. In brief, cells were seeded onto the upper side of the transwell inserts in serum-free DMEM and immediately treated with test substances or vehicles for the indicated times. DMEM (high glucose, GlutaMAX™) containing 10% (v/v) FCS

was used as chemoattractant in the companion plate. Following incubation at 37°C and 5% CO_2 atmosphere for 6 h (except time-course experiments in Fig. 1D, E), the nonmigrated cells on the upper surface of the inserts were removed with a cotton swab. For calculation of migration, the viability of the migrated cells on the lower side of the transwell insert was determined by the colorimetric 4-[3-(4-iodophenyl)-2-(4-nitrophenyl)-2H-5-tetrazolio]-1.6-benzene disulfonate (WST-1) test (Roche Applied Science, Mannheim, Germany). WST-1 tests were likewise performed in 96-well plates to exclude the possibility that promigratory actions of test substances were unspecific effects caused by increased cellular viability (Table 1).

Scratch wound healing assay

To visualize migration of cells, human MSCs were seeded into 24-well plates and allowed to grow for 24 h in DMEM containing 10% (v/v) FCS. A 100 µl plastic pipette tip was used for gently scratching the cell monolayer to create a cell-free area. Subsequently, cells were washed extensively with PBS to remove cellular debris. Thereafter, cells were incubated with URB597, AA-5HT, or vehicle in serum-free DMEM. Wound closure was monitored after 24 h (URB597) and 12 h (AA-5HT), respectively. Images of marked regions along the wounded area were obtained using an inverted microscope.

Fluorescence microscopy

MSCs were seeded in 4-well culture slides [BD Falcon™ CultureSlides (BD Biosciences)] at a density of 1×10^5 cells/well and grown overnight at 37°C in DMEM (high glucose, GlutaMAX™) supplemented with 10% (v/v) FCS, 100 U/ml penicillin, and 100 µg/ml streptomycin. After 24 h, the medium was changed and after an additional 24 h, cells were stimulated with the indicated test substances in serum-free DMEM. Test substances were prepared as described above (see Cell culture). Following incubation, cells were washed three times and fixed using 4% (v/v) paraformaldehyde. Fixation was performed for 1 h at room temperature or overnight at 4°C. Subsequently, cells were washed three times and blocked using a PBS solution containing 5% (v/v) FCS and 0.3% (v/v) Triton® X-100 for 1 h at room temperature. Following another washing step, cells were probed with an anti-PPARα antibody (Abcam, Bristol, UK) that was diluted 1:500 in PBS containing 1% (v/v) FCS and 0.3% (v/v) Triton® X-100 for 1 h at room temperature. Thereafter, cells washed with PBS were probed using an Alexa Fluor® 488 dye-conjugated goat anti-mouse IgG antibody (Life Technology Corporation, Darmstadt, Germany) at a dilution 1:1,000. This PBS solution additionally contained the DNA binding fluorescent dye bisbenzimide (4 µg/ml), 1% (v/v) FCS, and 0.3% (v/v) Triton® X-100. Antibody binding and nuclei detection were visualized by fluorescence microscopy using an Axioscope 1.A from Zeiss (Jena, Germany). Determination of nuclear PPARα was carried out by merging nuclear regions (bisbenzimide-stained areas) and Alexa Fluor® 488-labeled PPARα. Analysis of light intensities and quantification was achieved using the Zeiss Zen Pro 2012 analysis software.

Western blot analysis

Human MSCs were seeded into 6-well plates and grown to confluence. Western blot analyses were performed as described recently (33). Following incubation with test substances or vehicles for the indicated times, cells were lysed in solubilization buffer [50 mM HEPES (pH 7.4), 150 mM NaCl, 1 mM EDTA, 1% (v/v) Triton® X-100, 10% (v/v) glycerol, 1 mM PMSF, 1 µg/ml leupeptin, 0.5 mM orthovanadate, and 10 µg/ml aprotinin], homogenized by vigorous mixing for 30 min on ice, and centrifuged at 20,000 *g* for 5 min. Total protein concentration was measured using the bicinchoninic acid assay (Pierce®, Thermo Fisher Scientific, Bonn, Germany).

Proteins were separated on a 10% SDS polyacrylamide gel. Following transfer to nitrocellulose (Carl Roth GmbH) and blocking of the membranes with 5% milk powder, blots were probed with specific antibodies raised to β-actin (loading control; Sigma), p42/44 MAPK, or phospho-p42/44 MAPK (Cell Signaling Technology, Leiden, The Netherlands). Subsequently, membranes were probed with horseradish peroxidase-conjugated Fab-specific anti-mouse (for detection of β-actin) or anti-rabbit IgG (for detection of p42/44 MAPK and phospho-p42/44 MAPK, both secondary antibodies from Cell Signaling Technology). The following antibody dilutions were used: 1:10,000 (β-actin), 1:1,000 (p42/44 MAPK and phospho-p42/44 MAPK). Antibody binding was visualized using chemiluminescence solution containing 1.25 mM luminol, 200 µM para-cumaric acid, 0.09% (v/v) H_2O_2, and 0.0072% (v/v) DMSO in 100 mM Tris-HCl (pH 8.5). Densitometric analysis of band intensities was done by optical scanning and quantifying using the Quantity One 1-D analysis software (Bio-Rad Laboratories GmbH). Activation of p42/44 MAPK was calculated by normalizing densitometric values of blots exposed to phospho-specific antibodies to densitometric values of the bands obtained from blots exposed to the antibodies against the nonphosphorylated p42/44 MAPK. β-actin was used to visualize equal protein loading.

LC-MS analyses

MSCs were seeded in Petri dishes with a 10 cm diameter and grown at 37°C in DMEM (high glucose, GlutaMAX™) supplemented with 10% (v/v) FCS, 100 U/ml penicillin, and 100 µg/ml streptomycin. For one sample (vehicle or FAAH inhibitor) per donor, eight Petri dishes were used. After 24 h, the medium was replaced by fresh DMEM containing 10% (v/v) FCS and antibiotics and incubated for another 24 h. Subsequently, the cells were washed once with PBS and incubated for 3 h in serum-free DMEM. Thereafter cells were incubated in serum-free DMEM with vehicle, 10 µM URB597, or 10 µM AA-5TH for another 6 h. Subsequently, cells were harvested by scraping and cell pellets obtained after centrifugation (10 min, 2,000 *g*, 4°C) were frozen in liquid nitrogen and stored at −80°C prior to analysis. For the determination of endocannabinoids, cell pellets were further resuspended in 1 ml of 20 mM Tris-HCl buffer (pH 6.8) spiked with 20 ng/ml of AEA-d_8 and lysed using a Sonopols U-tip sonifier (Bandelin, Berlin, Germany) three times with a 15 × 5 s pulse at 75% power followed by a 60 s pause. The lysates were transferred to ice-cold screw-capped glass tubes. In parallel with standard solutions, samples were extracted and analyzed as described recently (51). Briefly, extracted samples (30–60 µl) were analyzed on a Waters HPLC 2695 separation module using a Multospher 120 C18 column 125 × 2 mm, 5 µm particle size (CS-Chromatographie Service GmbH, Langerwehe, Germany) coupled with a guard column (20 × 2 mm, 5 µm particle size). Endocannabinoids and endocannabinoid-like substances were resolved using mobile phase A (water containing 0.2% formic acid) and mobile phase B [acetonitrile/2-propanol (60:40, v/v) containing 0.2% formic acid] at a flow rate of 0.15 ml/min. The elution scheme was as follows: linear increase of the mobile phase B from 65% to 80% in 10 min, isocratic at 80% of phase B in 3 min and linearly to 100% phase B in the following 6 min. Finally, the system was reequilibrated at 35% phase A over 4 min. The HPLC column effluent was introduced into a Micromass Quatro Micro™ API mass spectrometer (Waters, Milford, MA) and analyzed using electrospray ionization in the positive mode and a single ion monitoring modus: *m/z* 300.8 for PEA, *m/z* 326.8 for OEA, *m/z* 348.8 for AEA, *m/z* 379.8 for 2-AG, and *m/z* 356.8 for the internal standard (AEA-d_8). The mass spectrometer and source parameters were set up as follows: capillary voltage, 3.5 kV; cone voltage, 20 and 24 V for AEA/AEA-d_8/2-AG and PEA/OEA, respectively; source temperature, 120°C; desolvation temperature, 350°C; flow

rate of desolvation gas, 700 l/h. Dwell and delay times were 0.05 and 0.1 s, respectively. All instrument parameters for the monitored analytes were tuned by injecting standard solutions at a concentration of 100 ng/ml at 10 μl/min flow rate by a syringe pump. The data were acquired using MassLynx software version 4.1 (Micromass Ltd., Manchester, UK). Upon quantitation, the signals obtained for each analyte were normalized to the amount of internal standard observed in the corresponding sample. No effect of additives (URB597 or AA-5HT) was observed during preparation of calibration curves for each of the standards used. Finally, an aliquot of each lysate (10 μl) was used for quantification of total protein using the bicinchoninic acid assay (Pierce®, Thermo Fisher Scientific).

Statistics

Comparisons between groups were performed with Student's 2-tailed *t*-test or with one-way ANOVA plus post hoc Bonferroni or Dunnett test using GraphPad Prism 5.04 (GraphPad Software, Inc., San Diego, CA). *P* values of less than 0.05 were considered significant.

RESULTS

Promigratory impact of FAAH inhibitors on MSCs

The effect of the FAAH inhibitors, URB597 and AA-5HT, on the migration of MSCs was determined using Boyden chambers. Time-course experiments revealed the promigratory effect of 10 μM URB597 to yield statistical significance following a 2 h incubation period (**Fig. 1A**), while 10 μM AA-5HT had already reached significance after a 1 h incubation (Fig. 1B). Following a 6 h incubation with either FAAH inhibitor, the migration of MSCs was increased in a concentration-dependent manner (Fig. 1C, D).

In addition, the promigratory action of both FAAH inhibitors was confirmed using the scratch wound healing assay. Accordingly, a 24 h (URB597) or 12 h (AA-5HT) incubation of MSCs with 10 μM of the respective FAAH inhibitor was associated with enhanced wound closure, as compared with vehicle-treated cells (Fig. 1E).

To rule out the possibility that enhanced migration of MSCs in response to URB597 and AA-5HT was an unspecific effect due to increased cellular viability, WST-1 tests were performed using a similar treatment protocol (see Migration assay). Interestingly, URB597- and AA-5HT-treated MSCs exhibited a tendency toward a decrease, rather than an increase, of viability, with cells exposed to URB597 even exhibiting a significant loss of viability. However, the loss of viability did not fall below a value of approximately 85% of the vehicle controls (100%) (**Table 1**, first two columns, left hand side).

Involvement of p42/44 MAPK in the promigratory effect of FAAH inhibitors

As demonstrated recently, p42/44 MAPK activation plays a crucial role in the signaling cascade conferring enhanced migration of MSCs (33). Based on this finding, URB597 and AA-5HT were tested for phoshorylation of p42/44 MAPK in Western blot analyses. Both FAAH inhibitors caused a time-dependent activation of p42/44 MAPK with URB597 yielding a significant peak phosphorylation following a 2 h incubation period (**Fig. 2A**), whereas MSCs exposed to AA-5HT already showed significant p42/44 MAPK activation after 30 min (Fig. 2B). MSCs exhibited a concentration-dependent activation of p42/44 MAPK when treated with URB597 for 2 h (Fig. 2C) or with AA-5HT for 1 h (Fig. 2D).

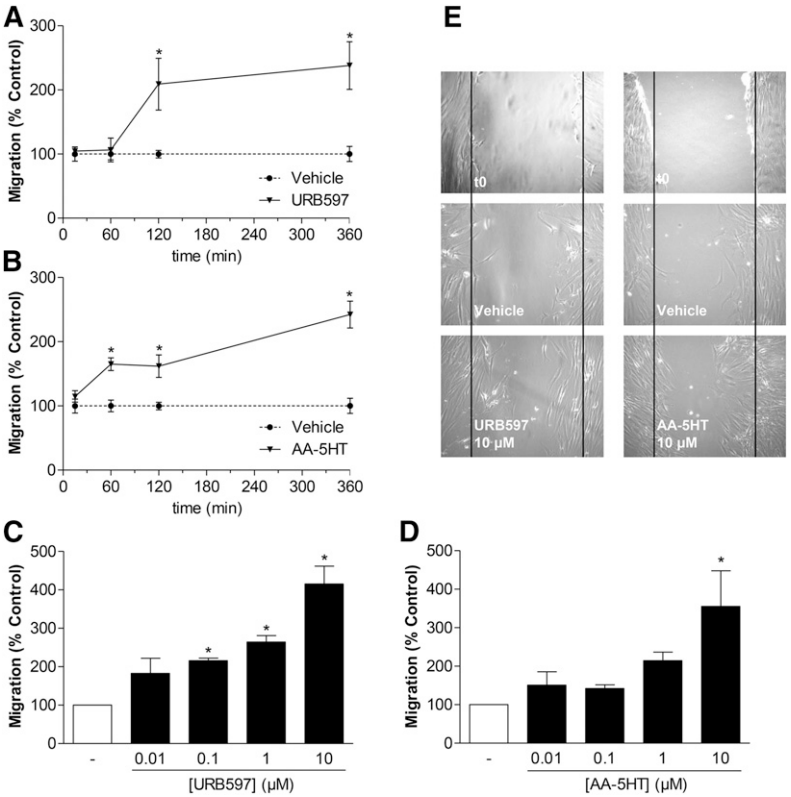

Fig. 1. Impact of the FAAH inhibitors URB597 and AA-5HT on the migration of MSCs. A, B: Time-course of migration of MSCs treated with vehicle, 10 μM URB597 (A), or 10 μM AA-5HT (B) in Boyden chamber assays. C, D: Concentration-dependent impact of URB597 and AA-5HT on migration of MSCs (Boyden chamber assays). MSCs were incubated with vehicle, URB597 (C), or AA-5HT (D) at the indicated concentrations for 6 h. E: Phase contrast images of migration of MCSs into scratched areas following a 24 h (URB597) or 12 h (AA-5HT) incubation with the respective FAAH inhibitor or its vehicle. The indicated images depict one representative experiment. t0, the untreated cells immediately after scratching the cells. Data represent mean ± SEM compared with vehicle controls (100%) of n = 3–4 experiments with cells from one donor (A, B), n = 6–7 experiments with cells from two donors (C, D; vehicle, 1 μM and 10 μM), and n = 3–4 experiments with cells from one donor (C, D; vehicle, 0.01 μM and 0.1 μM), respectively. With respect to different vehicle controls in (C) and (D) that were considered for statistical evaluation of the respective experiment, vehicle bars in (C) and (D) do not contain SEM. *$P < 0.05$; Student's *t*-test (A, B) and one-way ANOVA plus post hoc Dunnett test (C, D).

TABLE 1. Analysis of cellular viability of MSCs treated with FAAH inhibitors, endocannabinoids, and endocannabinoid-like substances

	Viability (%)					
Concentration (μM)	URB597	AA-5HT	AEA	2-AG	OEA	PEA
0	100.0 ± 1.2	100.0 ± 1.6	100.0 ± 4.0	100.0 ± 3.5	100.0 ± 3.6	100.0 ± 6.1
0.1	86.7 ± 1.7[a]	91.2 ± 3.2[a]	79.3 ± 7.6[b]	93.6 ± 9.7[b]	94.3 ± 4.9[b]	93.2 ± 6.3[b]
1	87.4 ± 1.6[a]	89.8 ± 2.9[a]	85.0 ± 7.8[b]	95.4 ± 7.9[b]	91.5 ± 5.1[b]	99.9 ± 5.6[b]
10	91.0 ± 1.6[a]	88.7 ± 2.5[a]	93.3 ± 3.7[b]	126.9 ± 9.0[b]	95.7 ± 5.1[b]	115.7 ± 4.3[b]

MSCs were treated with vehicle (line 0) or the indicated concentrations of test substances in serum-free DMEM for 6 h. Thereafter, viability was assessed by WST-1 test. Percent control represents mean ± SEM of n = 30 (URB597; five donors), n = 24 (AA-5HT; four donors), and n = 12 (AEA, 2-AG, OEA, and PEA; three donors) experiments.

[a] $P < 0.05$ versus corresponding vehicle, one-way ANOVA plus post hoc Dunnett test.

[b] Not significant versus corresponding vehicle, one-way ANOVA plus post hoc Dunnett test.

In an attempt to evaluate a causal link between the enhanced migration by FAAH inhibitors and their ability to induce p42/44 MAPK activation, the inhibitor of p42/44 MAPK activation, PD98059, was tested for its involvement in the promigratory impact of both FAAH inhibitors. To this end, MSCs were treated with vehicle or 10 μM URB597 and AA-5HT in the presence or absence of PD98059. Inhibition of p42/44 MAPK activation by PD98059 was associated with a significant reduction of migration caused by URB597 (Fig. 2E) and AA-5HT (Fig. 2F). In order to test a second member of the MAPK family for a possible involvement in the promigratory impact on MSCs, the p38 MAPK inhibitor, SB203580, was included in these experiments. However, inhibition of p38 MAPK left the promigratory effect of both FAAH inhibitors virtually unaltered (Fig. 2E, F).

FAAH inhibitors confer increased levels of AEA, 2-AG, OEA, and PEA in MSCs

To evaluate the inhibitory action of both FAAH inhibitors on the activity of FAAH that has been found to be expressed in MSCs from different donors as assessed by Western blot analyses (data not shown), MSCs were treated with URB597 and AA-5HT (both at 10 μM) for 6 h, respectively, and subsequently analyzed for FAAH substrates by LC-MS. As shown in **Fig. 3**, all of the analyzed FAAH substrates (AEA, 2-AG, OEA, and PEA) were found at higher intracellular concentrations when MSCs were treated with URB597 or AA-5HT, as compared with the respective vehicle. In experiments with cells from three different donors, AA-5HT was shown to exhibit the highest mean of AEA in MSCs, although the variation of response was most pronounced, as compared with the other evaluations. On the other hand, LC-MS analyses of cells from four different donors yielded higher levels of the endocannabinoid-like substances, OEA and PEA, in cells treated with URB597, as compared with AA-5HT. Notably, URB597 elicited only a weak increase of 2-AG, which is mainly catabolized by MAGL (4). The extraction procedure and HPLC conditions were designed to minimize undesirable isomerization of 2-AG (51). For the analysis shown in Fig. 3, only 2-AG was considered.

Collectively, these experiments suggest that FAAH degrades both endocannabinoids and endocannabinoid-like substances in MSCs, with all analyzed lipid mediators being increased upon inhibition of FAAH by URB597 and AA-5HT, respectively.

Increased migration and p42/44 MAPK activation by exogenously added AEA, 2-AG, OEA, and PEA

Based on the detected elevation of endocannabinoids and endocannabinoid-like substances in FAAH inhibitor-treated MSCs, a potential promigratory and p42/44 MAPK-activating effect of exogenously added AEA, 2-AG, OEA, and PEA was quantified next using Boyden chamber assays and Western blots, respectively.

Analysis of AEA, 2-AG, OEA, and PEA tested in a range of 0.1–10 μM at an incubation time of 6 h revealed a concentration-dependent promigratory impact on MSCs that was likewise abrogated in the presence of PD98059 for all test substances (**Fig. 4A–D**, left panels). Increased migration in response to endocannabinoids and endocannabinoid-like substances was associated with profound activation of p42/44 MAPK following a 2 h incubation with test substances at 10 μM (Fig. 4A–D, right panels). According to the indicated densitometric analyses, p42/44 MAPK activation by test substances used at 1 μM yielded means ± SEMs of 140 ± 18% (AEA), 150 ± 19% (OEA), and 138 ± 21% (PEA), as compared with the respective vehicle. Noteably, activation of p42/44 MAPK in response to 2-AG appeared as a threshold effect.

To rule out the possibility that a modulation of viability may confer an unspecific impact on the migratory behavior of MSCs, AEA, 2-AG, OEA, and PEA were evaluated for their influence on viability following a 6 h incubation period. According to Table 1 (four right columns), none of the FAAH substrates yielded a statistically significant alteration of viability. Interestingly, 2-AG at 10 μM elicited an increase of viability to 126.9% of control, and OEA at 10 μM increased viability to 115.7% of control. However, both effects did not reach statistical significance.

Involvement of cannabinoid receptors and TRPV1 in FAAH inhibitor- and endocannabinoid-induced migration

In a recent study from our group, the cannabinoid receptors, CB_1 and CB_2, as well as TRPV1, were detected by Western blot analyses of membrane fractions from human MSCs (33). To investigate a probable involvement of these cannabinoid-activated receptors in the observed promigratory action of FAAH inhibitors and endocannabinoids, MSCs were pretreated with antagonists to CB_1 (AM-251), CB_2 (AM-630), and TRPV1 (capsazepine) for 1 h. Receptor antagonists were used at a final concentration of 1 μM that has previously been demonstrated to be sufficient to modulate

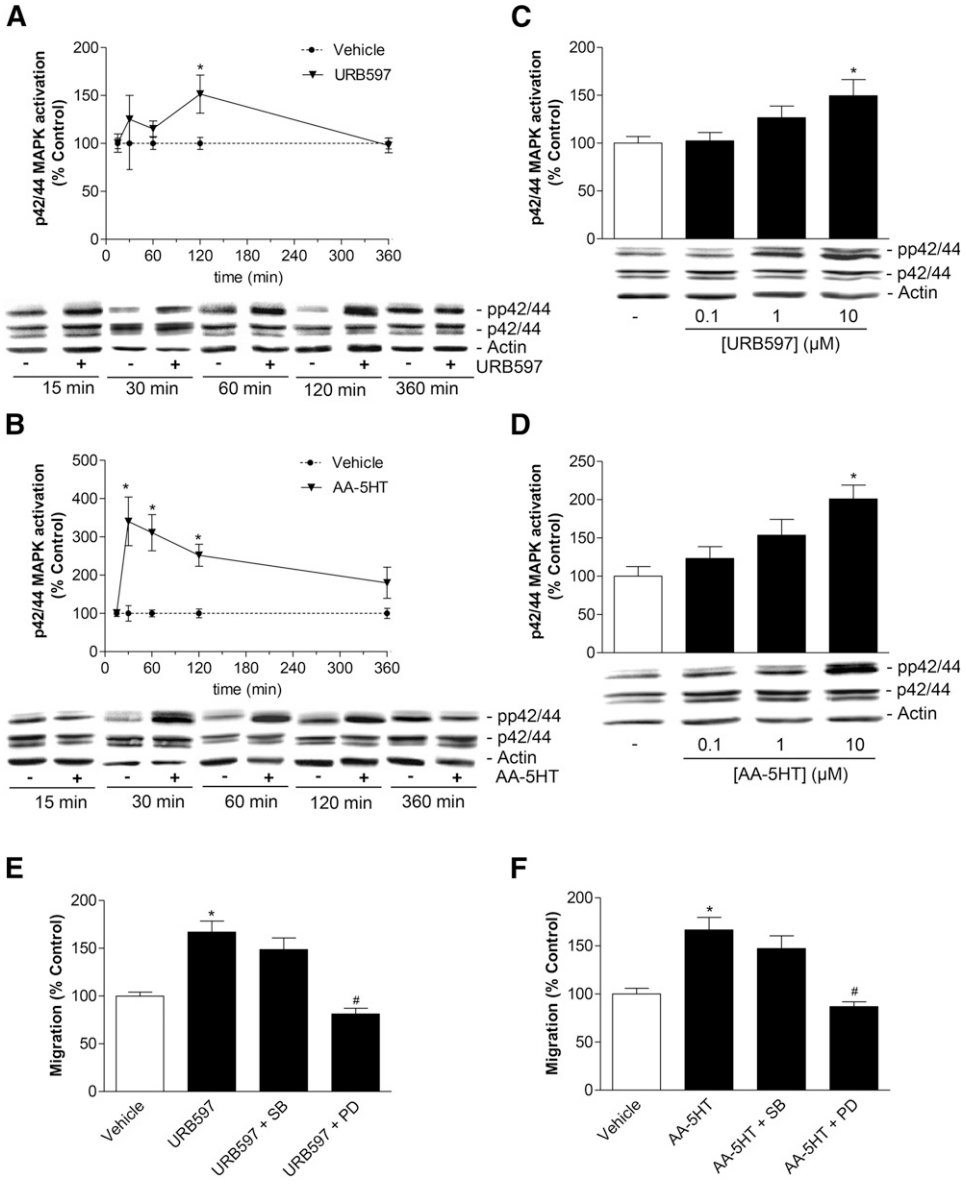

Fig. 2. Involvement of p42/44 MAPK in URB597- and AA-5HT-induced migration of MSCs. A, B: Time-course of p42/44 MAPK phosphorylation by URB597 (A) and AA-5HT (B) (Western blot analyses). Cells were treated with vehicle, 10 μM URB597 (A) or 10 μM AA-5HT (B), for the indicated times. C, D: Concentration-dependent activation of p42/44 MAPK by URB597 (C) and AA-5HT (D) (Western blot analyses). Cells were treated for 2 h (C, URB597) or 1 h (D, AA-5HT) with vehicle or the indicated concentrations of the test substances. To indicate activation of p42/44 MAPK, values obtained from densitometric band analyses of the phosphorylated form were normalized to those of nonphosphorylated p42/44 MAPK. β-actin was used as loading control. E, F: Analysis of FAAH inhibitor-induced promigratory effects in the presence of a p42/44 MAPK signaling pathway blocker and a p38 MAPK blocker. Cells were pretreated with the upstream inhibitor of p42/44 activation, PD98059 (PD, 10 μM), or the p38 MAPK inhibitor SB203580 (SB, 10 μM) for 1 h and subsequently incubated with vehicle, URB597 (E, 10 μM) or AA-5HT (F, 10 μM) for another 6 h before quantification of migration by Boyden chamber assays. Data represent mean ± SEM compared with vehicle control (100%) of n = 15 experiments with cells from five donors (A, 15 min and 360 min), n = 9 experiments with cells from three donors (A, 30 min), n = 21 experiments with cells from seven donors (A, 60 min and 120 min), n = 6 experiments with cells from two donors (B–D), n = 16 experiments with cells from four donors (E, F). $^{*}P < 0.05$ versus vehicle, Student's *t*-test (A, B) or one-way ANOVA plus post hoc Dunnett (C, D) or Bonferroni test (E, F). $^{\#}P < 0.05$ versus respective FAAH inhibitor in the absence of PD98059; one-way ANOVA plus post hoc Bonferroni test (E, F).

receptor activity (33, 52). URB597- and AA-5HT-induced migration was signifigantly abrogated in the presence of AM-630, suggesting the CB_2 receptor to functionally contribute to the observed effects (**Table 2**, rows 1–10). In addition, the promigratory effect of both FAAH inhibitors appeared to be fully reversed in the presence of a combination of antagonists to both CB_1 and CB_2 (Table 2, rows 1–10). Furthermore, the TRPV1 antagonist, capsazepine,

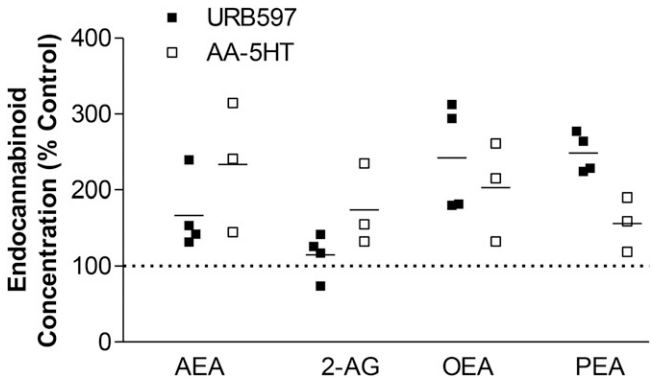

Fig. 3. Impact of the FAAH inhibitors URB597 and AA-5HT on levels of FAAH substrates in MSCs. Cells were treated with vehicle or FAAH inhibitors (10 μM) for 6 h. Concentrations of endocannabinoids and endocannabinoid-like substances were quantified from cell lysates by LC-MS. All concentrations were normalized to cellular protein amounts. Percent control refers to comparison with respective vehicle controls (100%). Vehicle controls of FAAH inhibitors are indicated as one dotted line in the scatter dot plot. For calculation of the respective percentage stimulation, the corresponding vehicle controls for URB597 (n = 4) and AA-5HT (n = 3) were used. Horizontal lines in the scatter dot plot indicate the respective mean of the indicated single experiments from n = 4 donors (URB597) or n = 3 donors (AA-5HT). Basal concentrations of FAAH substrates measured in vehicle-treated cells were 1.13 ± 0.29 pmol/mg protein (AEA), 24.62 ± 2.42 pmol/mg protein (2-AG), 6.20 ± 1.37 pmol/mg protein (OEA), and 4.13 ± 0.87 pmol/mg protein (PEA) (mean ± SEM from single experiments from n = 4 donors), respectively.

was found to cause complete inhibition of URB597-induced migration as well as AA-5HT-induced migration (Table 2, rows 11–16). It is noteworthy that capsazepine, itself, elicited inhibition of basal migration when MSCs were treated with capsazepine alone (Table 2, row 16), which is in line with recent data from our group (33). As expected from these results, AM-630 and capsazepine furthermore significantly inhibited the promigratory impact of AEA and 2-AG on MSCs (Table 2, rows 17–28). As further shown in Table 2 (rows 1–10 and rows 17–28), the CB_1 antagonist, AM-251, also lowered the promigratory impact of both FAAH inhibitors and endocannabinoids without yielding statistical significance. Accordingly, the combination of AM-251 and AM-630 elicited a more pronounced inhibition of the URB597-, AA-5HT-, AEA-, and 2-AG-induced migration, as compared with the effect of AM-630 alone.

Involvement of PPARα in the promigratory effect of URB597, AA-5HT, AEA, 2-AG, OEA, and PEA

To elucidate a possible contribution of PPARα to the promigratory action of URB597 and AA-5HT, the impact of the selective PPARα antagonist, GW6471, on migration of MSCs using Boyden chamber assays was analyzed next. Increases of MSC migration caused by both FAAH inhibitors were completely reversed by the PPARα antagonist, GW6471 (**Fig. 5A**). In line with this finding, the endocannabinoids, AEA and 2-AG, were likewise found to elicit their inductive effect on MSC migration in a GW6471-sensitive manner (Fig. 5B). Similar results could be proven for the endocannabinoid-like substances OEA (Fig. 5C) and PEA (Fig. 5D). Here, the TRPV1 antagonist, capsazepine, was additionally tested for its impact on the promigratory effect of both fatty acid amides, as was also done with the other test substances (see Table 2). As shown in Fig. 5C, D, capsazepine led to an inhibition of the OEA- and PEA-induced migration of MSCs. Moreover, the concentration-dependent induction of migration by both FAAH inhibitors (Fig. 1C, D) and FAAH substrates (Fig. 4A–D, left panels) was mimicked by the synthetic PPARα agonist, WY-14643 (Fig. 5E).

Influence of p42/44 MAPK inhibition on PPARα activation by URB597, AA-5HT, AEA, 2-AG, OEA, and PEA

In an attempt to confirm an activation of PPARα by FAAH inhibitors and substrates, fluorescence microscopy using a PPARα antibody visualized by a Alexa Fluor® 488 dye-tagged secondary antibody and a DNA binding fluorescent dye, bisbenzimide, was performed next to detect the nuclear accumulation of PPARα. Noteably, subcellular distribution of PPARα toward nuclear accumulation has been described as a reliable marker of PPARα activation (53). To provide evidence for a causal relationship between PPARα activation and p42/44 MAPK phosphorylation, analysis of nuclear accumulation of PPARα in the presence or absence of the p42/44 MAPK upstream inhibitor, PD98059, was carried out. According to **Fig. 6A**, 10 μM URB597 caused an increase of PPARα in the nuclei of MSCs that was significantly inhibited by PD98059, thereby confirming an involvement of p42/44 MAPK activation in this response. As a control, the PPARα antagonist, GW6471, also conferred an inhibition of the cytosol-to-nucleus translocation of PPARα. Comparable results were found in experiments using MSCs that were treated with 10 μM AA-5HT for 2 h (Fig. 6B).

In order to evaluate whether the FAAH substrates that are upregulated upon treatment of MSCs with URB597 and AA-5HT also cause a p42/44 MAPK-dependent PPARα activation, AEA, 2-AG, OEA, and PEA were tested using the same experimental setting. In fact, 10 μM AEA (**Fig. 7A**) and 2-AG (Fig. 7B) induced a cytosol-to-nuclear translocation of PPARα that was likewise inhibited by upstream inhibition of p42/44 MAPK activation with PD98059 and by the PPARα antagonist. Similar results were further proven for OEA (Fig. 7C) and PEA (Fig. 7D).

It is noteworthy that PD98059 alone did not significantly alter PPARα accumulation in the nucleus, as compared with vehicle control [114.8 ± 4.9%, $P > 0.05$ for 10 μM PD98059 vs. vehicle (100 ± 3.4%) (mean ± SEM)]. On the other hand, in the same experiment the PPARα agonist WY-14643 conferred significant nuclear PPARα accumulation [137.5 ± 7.7%, $P < 0.001$ for 50 μM WY-14643 vs. vehicle (100 ± 3.4%) (mean ± SEM), one-way ANOVA plus post hoc Bonferroni test of n = 96 nuclei (vehicle), n = 99 nuclei (PD98059), and n = 102 nuclei (WY-14643) from cells of three donors]. In a separate experiment, the PPARα antagonist, GW6471, left basal PPARα translocation to the nuclei virtually unaltered [95.9 ± 1.7%, $P > 0.05$ for 10 μM GW6471 vs. vehicle (100% ± 1.1%) (mean ± SEM), Student's *t*-test of n = 42 nuclei for vehicle and GW6471 from cells of one donor].

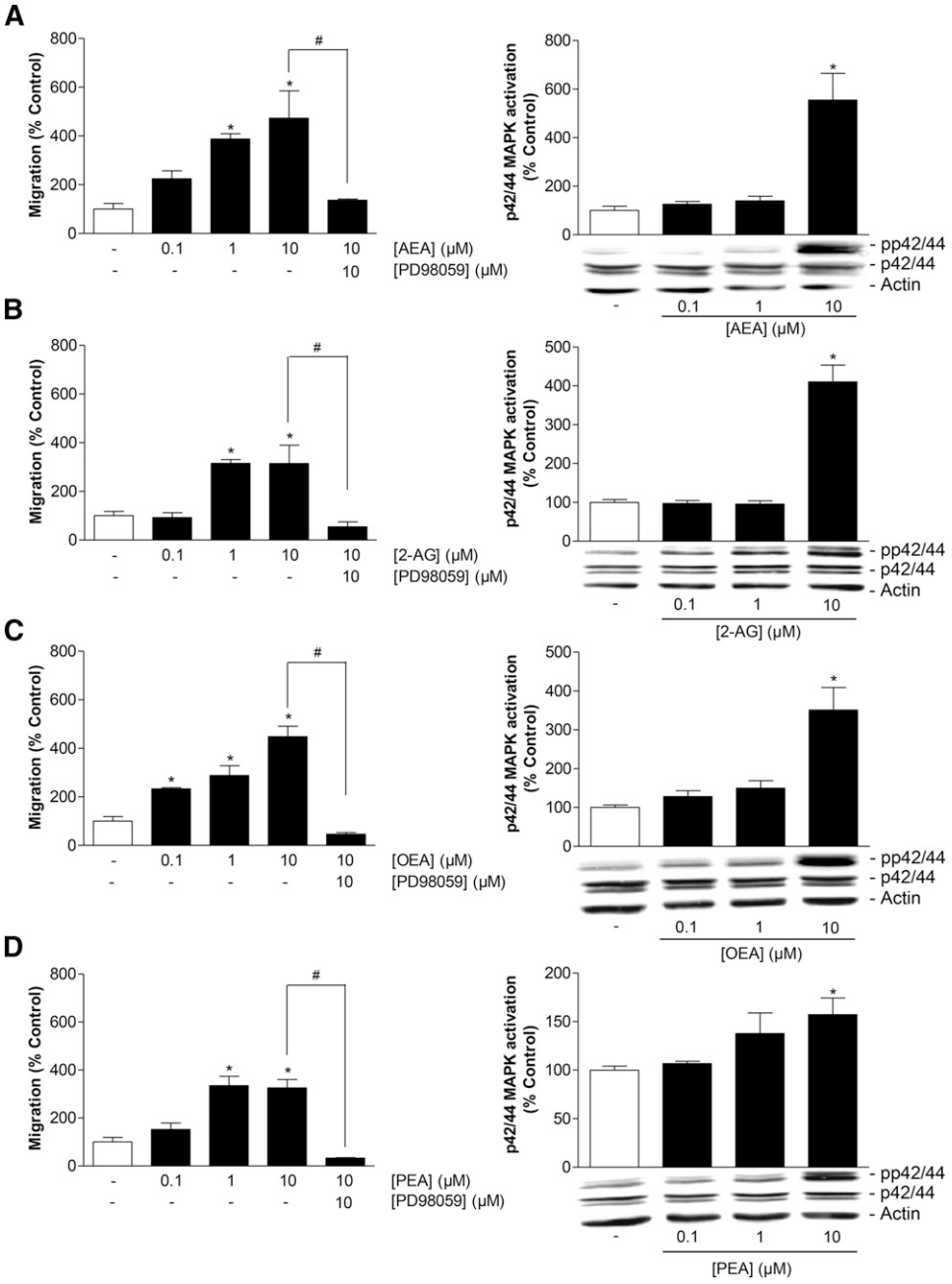

Fig. 4. Impact of endocannabinoids and endocannabinoid-like substances on migration and p42/44 MAPK activation in MSCs. A–D (left panels): Concentration-dependent effects of AEA (A), 2-AG (B), OEA (C), and PEA (D) on migration of MSCs (Boyden chamber assays) following a 6 h incubation period with vehicle or the indicated concentration of test substances and impact of the p42/44 MAPK activation inhibitor PD98059 (1 h pretreatment) on the promigratory action of 10 μM of the respective test compound. A–D (right panels): Concentration-dependent effects of AEA (A), 2-AG (B), OEA (C), and PEA (D) on p42/44 MAPK phosphorylation in MSCs (Western blots) following a 2 h incubation period with vehicle or the indicated concentrations of test substances. β-actin was used as loading control. Histograms above the blots indicate activation of p42/44 MAPK determined by densitometric analyses of phosphorylated p42/44 MAPK normalized to that of nonphosphorylated p42/44. Percent control represents mean ± SEM compared with vehicle controls (100%) of n = 3 experiments using cells from one donor [left panels (A–D); right panel (B)] or n = 6 experiments using cells from two donors [right panels (A, C, D)]. $^{*}P < 0.05$ versus vehicle; $^{\#}P < 0.05$ as indicated, one-way ANOVA plus post hoc Bonferroni (left panels) or Dunnett test (right panels).

Influence of the PPARα antagonist, GW6471, on p42/44 MAPK activation by URB597, AA-5HT, AEA, 2-AG, OEA, and PEA

According to the data presented in Figs. 6, 7, inhibition of p42/44 MAPK activation counteracts PPARα translocation by FAAH inhibitors and FAAH substrates, thereby suggesting the p42/44 MAPK phosphorylation to occur upstream to PPARα activation by the test substances. To strengthen this notion, additional Western blot experiments were carried out to investigate the impact of PPARα inhibition on

TABLE 2. Involvement of cannabinoid-activated receptors in the promigratory action of FAAH inhibitors and endocannabinoids

Treatment groups	Migration (% Control)
Vehicle	100.0 ± 21.1
URB597	414.3 ± 27.0[a]
URB597 + AM-251	312.0 ± 43.0[b]
URB597 + AM-630	151.7 ± 20.3[c]
URB597 + AM-251 + AM-630	118.3 ± 12.4[c]
Vehicle	100.0 ± 20.0
AA-5HT	599.3 ± 35.3[a]
AA-5HT + AM-251	486.7 ± 40.7[b]
AA-5HT + AM-630	272.7 ± 32.1[c]
AA-5HT + AM-251 + AM-630	92.7 ± 13.7[c]
Vehicle	100.0 ± 5.8
URB597	335.5 ± 56.4[a]
URB597 + Capsa	51.3 ± 13.1[c]
AA-5HT	454.5 ± 80.2[a]
AA-5HT + Capsa	44.0 ± 13.6[c]
Capsa	68.0 ± 4.0
Vehicle	100.0 ± 24.6
AEA	229.5 ± 30.5[a]
AEA + AM-251	180.3 ± 10.6[b]
AEA + AM-630	129.3 ± 8.5[c]
AEA + AM-251 + AM-630	127.8 ± 11.0[c]
AEA + Capsa	95.0 ± 3.8[c]
Vehicle	100.0 ± 9.1
2-AG	240.3 ± 35.9[a]
2-AG + AM-251	170.0 ± 19.2[b]
2-AG + AM-630	157.5 ± 8.9[c]
2-AG + AM-251 + AM-630	66.5 ± 2.5[c]
2-AG + Capsa	138.3 ± 16.4[c]

MSCs were pretreated for 1 h with AM-251 (CB_1 antagonist), AM-630 (CB_2 antagonist), or capsazepine (Capsa) (TRPV1 antagonist) at 1 μM concentrations prior to addition of vehicle, FAAH inhibitors (URB597 and AA-5HT; 10 μM), or endocannabinoids (AEA and 2-AG; 10 μM) and incubation for another 6 h. Percent control represents mean ± SEM compared with vehicle control (100%) of n = 3–4 experiments from one donor.

[a] $P < 0.05$ versus corresponding vehicle.

[b] Not significant versus corresponding vehicle.

[c] $P < 0.05$ versus cells treated with the respective FAAH inhibitor or endocannabinoid, one-way ANOVA plus post hoc Bonferroni test.

p42/44 MAPK activation. As expected, these experiments revealed the URB597-induced p42/44 MAPK activation to be insensitive to preincubation with the PPARα antagonist, GW6471 (**Fig. 8A**). AA-5HT-induced p42/44 MAPK activation in MSCs was slightly inhibited by GW6471, but did not yield statistical significance (Fig. 8B). Finally and in agreement with this data, Western blot experiments with MSCs treated with AEA, 2-AG, OEA, and PEA revealed no impact of GW6471 on the activation of p42/44 MAPK by the four FAAH substrates (Fig. 8C, left panel). GW6471 did not significantly influence basal p42/44 MAPK phosphorylation in the absence of test substance (Fig. 8C, right panel).

DISCUSSION

The present study provides first-time proof for induction of migration of MSCs by FAAH inhibitors, endocannabinoids, and endocannabinoid-like substances. As the underlying pathway, a phosphorylation of p42/44 MAPK followed by activation of PPARα was identified (**Fig. 9**).

There are several lines of evidence supporting this mechanism. First, the promigratory action of both FAAH inhibitors (URB597 and AA-5HT) and FAAH substrates (i.e., the endocannabinoids, AEA and 2-AG, as well as the endocannabinoid-like substances, OEA and PEA) was completely reversed by PD98059, an inhibitor of p42/44 MAPK activation. In line with this notion, the increase of migration by either substance was accompanied by significant elevations of p42/44 MAPK phosphorylation. The inhibitory impact of FAAH inhibitors on their target enzyme was proven by LC-MS analysis that revealed increased levels of all four FAAH substrates in MSCs as a response to both FAAH inhibitors. Second, inhibitor as well as fluorescence microscopy approaches indicate an activation of the transcription factor, PPARα, to be involved in the promigratory response of MSCs upon treatment with FAAH inhibitors and their substrates. These findings were corroborated by use of the PPARα agonist, WY-14643, that mimicked a concentration-dependent stimulation of migration, as well as a nuclear accumulation of PPARα under the same experimental conditions. Third, evidence for a causal relationship between p42/44 MAPK phosphorylation and subsequent PPARα activation was provided by experiments showing PD98059 to inhibit an increase of PPARα in the nuclei of MSCs treated with URB597 and AA-5HT as well as FAAH substrates, thus confirming an involvement of p42/44 MAPK in PPARα activation.

Our data are in agreement with reports demonstrating the promigratory effect of cannabinoids on human corneal epithelial (31) and embryonic kidney cells (54) to be mediated via p42/44 MAPK activation. Likewise, the nonpsychoactive phytocannabinoid, cannabidiol, was recently found to confer increased migration of human MSCs via a pathway involving p42/44 MAPK (33).

PPARs represent phosphoproteins whose transcriptional activity can be modulated via phosphorylation by MAPKs [for review see (55)]. The inhibition of PPARα activation by blockade of the p42/44 MAPK pathway, as shown here, is corroborated by several other studies. For example, insulin was previously demonstrated to confer increased PPARα activity via prior activation of p42/44 MAPK (56) with the insulin-induced transactivation being due to phosphorylation of two serines (positions 12, 21) in the A/B domain of human PPARα (57).

In the present study, treatment of MSCs with the PPARα inhibitor, GW6471, did not significantly interfere with p42/44 MAPK activation by FAAH inhibitors and substrates, thereby excluding phosphorylation of p42/44 MAPK by the test substances to occur downstream to PPARα activation. This control experiment was initiated on the basis of spare, but existing, data indicating PPARs to control kinase-linked receptor signaling on different levels, such as by interfering with the phosphorylation cascade or with transcription factor binding on DNA [for review see (58)].

In agreement with the PPARα-mediated effects of FAAH inhibitors and substrates reported here, several other studies confirmed PPARα-dependent effects for either group of substances. First evidence of cannabinoid interaction with PPARα was published by Kozak et al. (12), who showed that 15-hydroxyeicosatetraenoic acid glyceryl ester, a

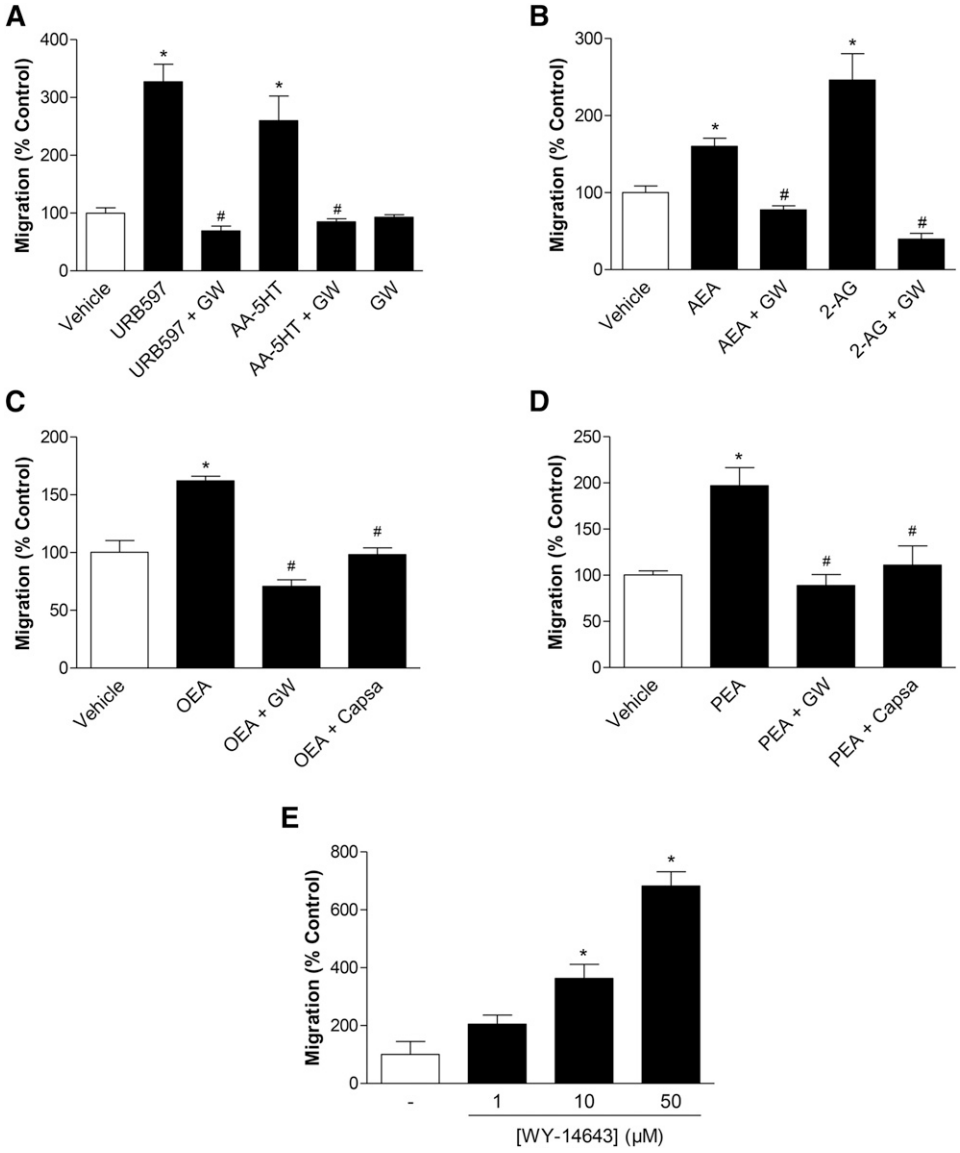

Fig. 5. Involvement of PPARα and TRPV1 in the promigratory effect of URB597, AA-5HT, endocannabinoids, and endocannabinoid-like substances on MSCs. A–D: MSCs were pretreated with the PPARα antagonist, GW6471 (GW) (10 μM), for 1 h and subsequently incubated with vehicle or the FAAH inhibitors URB597 and AA-5HT (A) (10 μM each), the endocannabinoids AEA and 2-AG (B) (10 μM each), or the endocannabinoid-like substances OEA (C) and PEA (D) (10 μM each) for another 6 h. In the case of OEA (C) and PEA (D), cells were likewise pretreated with the TRPV1 antagonist, capsazepine (Capsa, 1 μM), for 1 h. E: Concentration-dependent increase of migration by PPARα activation. MSCs were incubated with the selective PPARα agonist, WY-14643, at the indicated concentrations for 6 h. In all experiments, migration was assessed by Boyden chamber assays. Percent control represents mean ± SEM in comparison to vehicle-treated cells (100%) of n = 4 (A–D) or n = 3–4 (E) experiments using cells obtained from one donor. $^{*}P < 0.05$ versus vehicle; $^{\#}P < 0.05$ versus respective test substance in the absence of antagonists, one-way ANOVA plus post hoc Bonferroni (A–D) or Dunnett test (E).

metabolite of 2-AG generated upon metabolism via 15-lipoxygenase, acts as a PPARα agonist. Thereafter, OEA was demonstrated to confer appetite suppression and weight loss (10) and lipolysis (11), as well as neuroprotection (15), through activation of PPARα. Likewise, PEA was reported to exert anti-inflammatory and analgesic effects via PPARα (13). AEA, an endocannabinoid with PPARα binding and transcription activity (16), was recently reported to mediate relaxation of ophthalmic arteries in a PPARα-dependent manner (14). In consequence, various effects of FAAH inhibitors in animal experiments, including enhancement of memory acquisition (20), antinociception (17, 21), and blockade of nicotine reward and relapse (18), have been associated with activation of PPARα.

Remarkably, our experiments with the inhibitor of p42/44 MAPK activation, PD98059, revealed the phosphorylation of p42/44 MAPK as a crucial regulator of PPARα activation for all tested FAAH inhibitors and substrates. Thus, besides a direct PPARα binding, as previously shown by Sun et al.

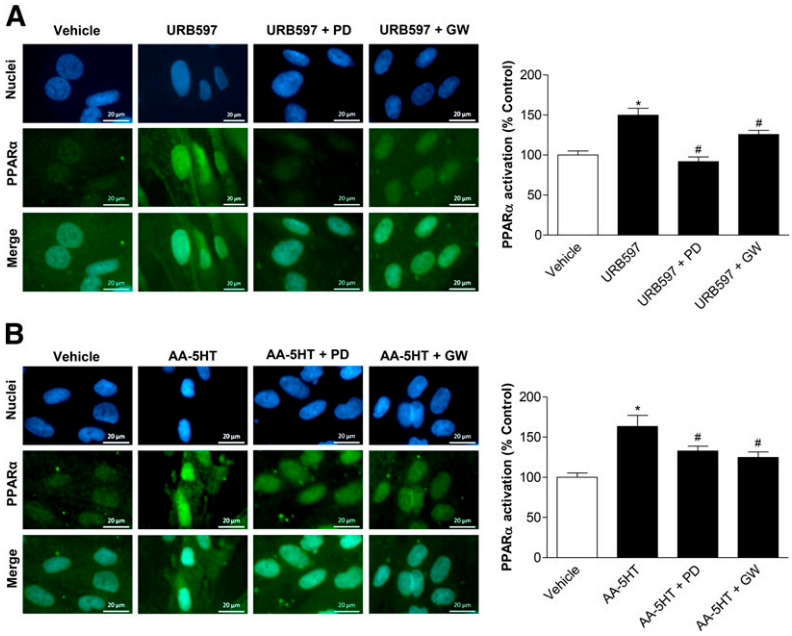

Fig. 6. Impact of p42/44 MAPK on URB597- and AA-5HT-induced PPARα activation. A, B: MSCs were pretreated with the upstream inhibitor of p42/44 MAPK activation, PD98059 (10 μM), or the PPARα antagonist, GW6471 (GW) (10 μM), for 1 h and subsequently incubated with URB597 (A, 10 μM) or AA-5HT (B, 10 μM) for another 2 h. PPARα activation was quantified by measuring colocalization of PPARα and nuclear regions of MSCs. Immunocytochemical staining of PPARα was carried out by hybridiziation of fixed cells with a PPARα antibody and subsequent staining using an Alexa Fluor® 488 dye-conjugated anti-mouse IgG secondary antibody. Nuclear regions were visualized by the DNA intercalating fluorescent dye, bisbenzimide. Nuclear PPARα was quantified by merging nuclear regions with PPARα fluorescence intensity. For quantitative analyses of PPARα detected in nuclear regions, fluorescence at 488 nm excitation of n = 45–65 nuclei (A, two donors) or n = 44–51 nuclei (B, two donors) was measured using the Zeiss Zen Pro 2012 analysis software. Pictures show representative images of nuclear regions (blue), PPARα (green), and PPARα merged to nuclei, respectively. Percent control represents PPARα fluorescence in nuclear regions indicated as mean ± SEM in comparison to vehicle-treated cells (100%) in the absence of test substances using cells obtained from one donor. $^{*}P < 0.05$ versus vehicle control; $^{\#}P < 0.05$ versus the respective FAAH inhibitor in the absence of antagonists, one-way ANOVA plus post hoc Bonferroni test.

(16) using a *cis*-parinaric acid-based ligand-binding system and a transient transfection system, additional mechanisms of PPARα activation appear feasible.

Apparently contradictory results have been published on the influence of PPARα on migration. In support of the data presented here, an increase of migration by PPARα activation was observed in human circulating angiogenic cells (59) and monocytic U937 cells (60). Interestingly, in the latter publication, the same PPARα agonist as that used in the present study (WY-14643) conferred increased migration of human monocytes, while a PPARγ agonist elicited the opposite effect. However, in other systems, including human airway smooth muscle cells (61) and human umbilical vein endothelial cells (62), PPARα activators have been reported to decrease migration. These results suggest that PPARα regulates migration in a cell- and stimulus-dependent manner with mechanisms still being poorly understood. Referring to the mechanism underlying PPARα-induced migration, a recent study found a reversal of PPARα-induced migration of circulating angiogenic cells by an Akt inhibitor (59).

Regarding the receptors conferring promigratory effects of cannabinoids on cells of the mesenchymal niches, CB_2 receptor activation by the CB_2 selective agonist, HU308, has been shown to increase the migration of murine osteoblast-like cells (44). Moreover, the nonpsychoactive cannabinoid, cannabidiol, was recently demonstrated to mediate increased migration of MSCs via activation of the CB_2 receptor (32). In line with this notion, an inhibitor approach in the present study yielded both FAAH inhibitors and CB receptor-active endocannabinoids (AEA and 2-AG) to confer increased migration, at least in part, via activation of CB_2. In addition, evidence was provided for a contribution of TRPV1 in increased migration by all FAAH inhibitors and FAAH substrates tested, which is in agreement with the reported TRPV1 activation by AEA (8), 2-AG (9), OEA (6), and PEA (7). Accordingly, the TRPV1 antagonist, capsazepine, blocked the promigratory actions in a partial (2-AG) and complete manner (URB597, AA-5HT, AEA, OEA, and PEA), respectively. However, interpretation of this data is hampered by the fact that capsazepine even diminished basal migration of MSCs, which is in agreement with the data published by Schmuhl et al. (33).

Another aspect that merits special consideration is that the levels of FAAH substrates were measured in cell lysates and were therefore necessarily indicated as picomoles per milligram of cellular protein. Thus, it was not possible to compare endogenous levels to the concentrations of exogenously added AEA, 2-AG, OEA, and PEA.

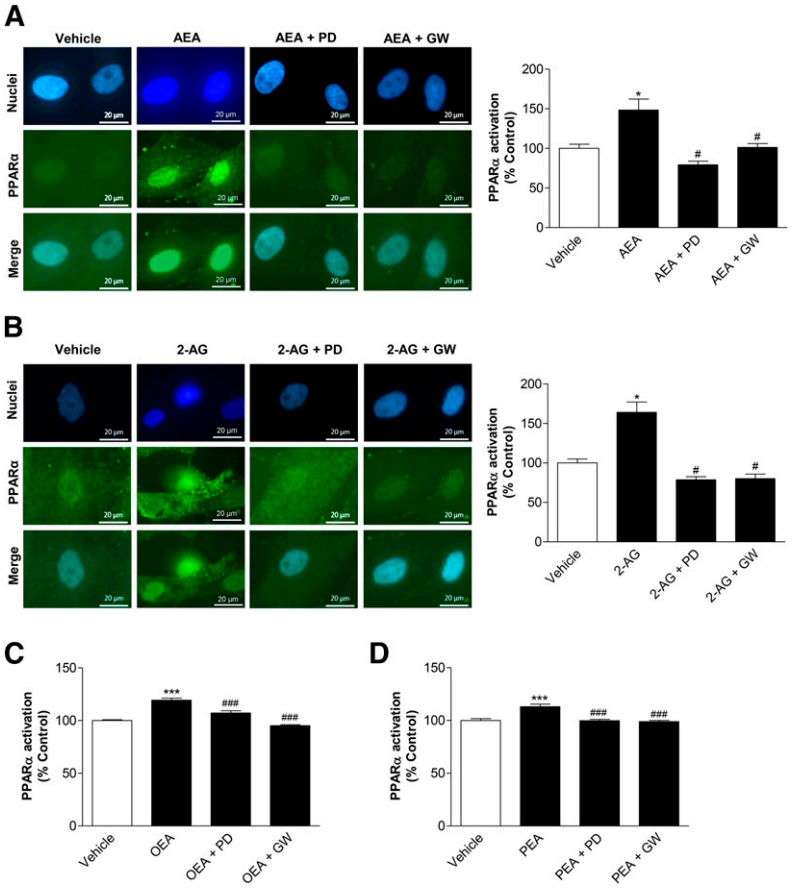

Fig. 7. Impact of p42/44 MAPK on PPARα activation by endocannabinoids and endocannabinoid-like substances. A, B: MSCs were pretreated with the upstream inhibitor of p42/44 MAPK activation, PD98059 (PD) (10 μM), or the PPARα antagonist, GW6471 (GW) (10 μM), for 1 h and subsequently incubated with AEA (A, 10 μM) or 2-AG (B, 10 μM) for another 2 h. PPARα activation was quantified by measuring colocalization of PPARα and nuclear regions of MSCs. Nuclear regions were visualized by the DNA intercalating fluorescent dye, bisbenzimide. Nuclear PPARα was quantified by merging nuclear regions with PPARα fluorescence intensity. Pictures at the left show representative images of nuclear regions (blue), PPARα (green), and PPARα merged with nuclei, respectively. C, D: Experiments for evaluation of the influence of PD98059 and GW6471 on OEA-induced (C) or PEA-induced (D) PPARα activation were carried out using the same protocols as (A) and (B). For quantitiative evaluation of nuclear PPARα, fluorescence at 488 nm excitation of n = 40–43 (A), n = 13–18 (B), n = 46 (C), or n = 24 (D) nuclei was measured using the Zeiss Zen Pro 2012 analysis software. Percent control represents PPARα fluorescence in nuclear regions indicated as mean ± SEM in comparison to vehicle-treated cells (100%) in the absence of test substances using cells obtained from one donor. $^{*}P < 0.05$ versus vehicle control; $^{\#}P < 0.05$ versus the respective endocannabinoid (A, B) or endocannabinoid-like substance (C, D) in the absence of antagonists, one-way ANOVA plus post hoc Bonferroni test.

Collectively, this is the first study to provide evidence for and insights into the promigratory action of inhibitors of FAAH and its substrates on human MSCs. The findings may offer a novel field of future in vivo investigations aimed at the regenerative effects of FAAH inhibitors which, according to animal experiments, already proved to be effective at ameliorating signs of acute, inflammatory, visceral, and neuropathic pain, and, in the case of URB597, signs of osteoarthritic pain [for review see (2)]. According to the data of the present study, endocannabinoids and endocannabinoid-like substances, whose concentrations may be pharmacologically enhanced by FAAH inhibitors, may impact the migratory action of stem cells of the mesenchymal niches in vivo, thereby contributing to tissue regeneration.

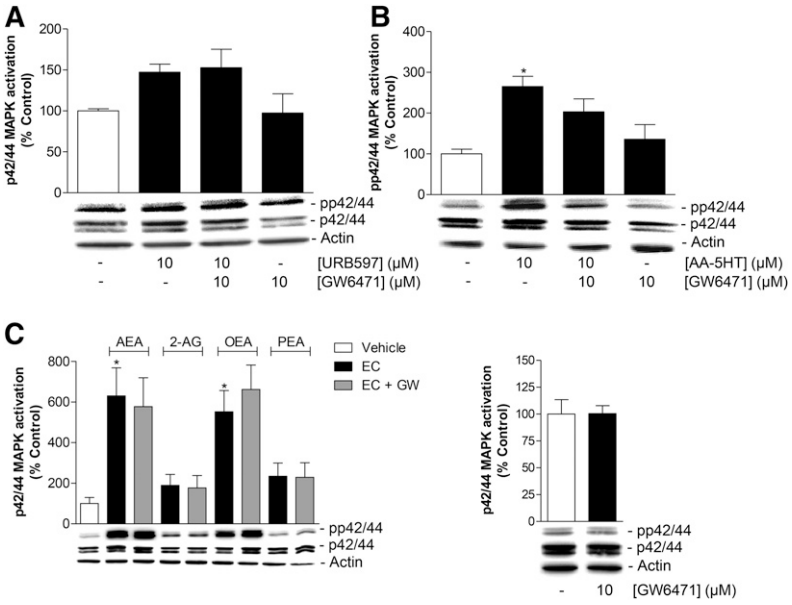

Fig. 8. Role of PPARα in FAAH inhibitor-induced, endocannabinoid-induced, or endocannabinoid-like substance-induced p42/44 MAPK activation. A, B: MSCs were pretreated with the PPARα antagonist GW6471 (10 μM) for 1 h and subsequently incubated with vehicle, URB597 (A; 10 μM, additional 2 h treatment) or AA-5HT (B; 10 μM, additional 1 h treatment). C: MSCs were pretreated with the PPARα antagonist GW6471 (GW) (10 μM) for 1 h and subsequently incubated with vehicle or the indicated endocannabinoids or endocannabinoid-like substances (EC) [AEA, 2-AG, OEA, or PEA (all at 10 μM)] for an additional 1 h incubation period. Histograms above the blots indicate activation of p42/44 MAPK determined by densitometric analyses of phosphorylated p42/44 MAPK normalized to that of nonphosphorylated p42/44 MAPK. β-actin was used as loading control. Data represent mean ± SEM compared with vehicle control (100%) of n = 5 experiments with cells from three donors (A), n = 6 experiments with cells from two donors (B), n = 6 experiments with cells from three donors (C, left panel), n = 6 experiments with cells from two donors (C, right panel). $^{*}P < 0.05$ versus vehicle, one-way ANOVA plus post hoc Bonferroni test.

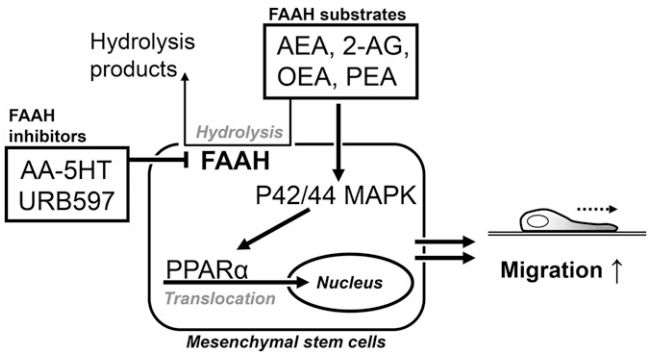

Fig. 9. Inhibition of FAAH by URB597 and AA-5HT causes increased levels of endocannabinoids and endocannabinoid-like substances in MSCs. As a consequence, these FAAH substrates induce activation of p42/44 MAPK that subsequently enhances PPARα translocation to the nucleus thereby conferring increased cellular migration.

REFERENCES

1. Di Marzo, V., and S. Petrosino. 2007. Endocannabinoids and the regulation of their levels in health and disease. *Curr. Opin. Lipidol.* **18:** 129–140.
2. Pertwee, R. G. 2014. Elevating endocannabinoid levels: pharmacological strategies and potential therapeutic applications. *Proc. Nutr. Soc.* **73:** 96–105.
3. Deutsch, D. G., and S. A. Chin. 1993. Enzymatic synthesis and degradation of anandamide, a cannabinoid receptor agonist. *Biochem. Pharmacol.* **46:** 791–796.
4. Blankman, J. L., G. M. Simon, and B. F. Cravatt. 2007. A comprehensive profile of brain enzymes that hydrolyze the endocannabinoid 2-arachidonoylglycerol. *Chem. Biol.* **14:** 1347–1356.
5. Saghatelian, A., S. A. Trauger, E. J. Want, E. G. Hawkins, G. Siuzdak, and B. F. Cravatt. 2004. Assignment of endogenous substrates to enzymes by global metabolite profiling. *Biochemistry.* **43:** 14332–14339.
6. Ahern, G. P. 2003. Activation of TRPV1 by the satiety factor oleoylethanolamide. *J. Biol. Chem.* **278:** 30429–30434.
7. Ambrosino, P., M. V. Soldovieri, C. Russo, and M. Taglialatela. 2013. Activation and desensitization of TRPV1 channels in sensory neurons by the PPARα agonist palmitoylethanolamide. *Br. J. Pharmacol.* **168:** 1430–1444.
8. Wisnoskey, B. J., W. G. Sinkins, and W. P. Schilling. 2003. Activation of vanilloid receptor type I in the endoplasmic reticulum fails to activate store-operated Ca^{2+} entry. *Biochem. J.* **372:** 517–528.
9. Zygmunt, P. M., A. Ermund, P. Movahed, D. A. Andersson, C. Simonsen, B. A. G. Jonsson, A. Blomgren, B. Birnir, S. Bevan, A. Eschalier, et al. 2013. Monoacylglycerols activate TRPV1–a link between phospholipase C and TRPV1. *PLoS One.* **8:** e81618.
10. Fu, J., S. Gaetani, F. Oveisi, J. Lo Verme, A. Serrano, F. R. de Fonseca, A. Rosengarth, H. Luecke, B. Di Giacomo, G. Tarzia, et al. 2003. Oleylethanolamide regulates feeding and body weight through activation of the nuclear receptor PPAR-alpha. *Nature.* **425:** 90–93.
11. Guzmán, M., J. Lo Verme, J. Fu, F. Oveisi, C. Blázquez, and D. Piomelli. 2004. Oleoylethanolamide stimulates lipolysis by activating the nuclear receptor peroxisome proliferator-activated receptor alpha (PPAR-alpha). *J. Biol. Chem.* **279:** 27849–27854.
12. Kozak, K. R., R. A. Gupta, J. S. Moody, C. Ji, W. E. Boeglin, R. N. DuBois, A. R. Brash, and L. J. Marnett. 2002. 15-Lipoxygenase metabolism of 2-arachidonylglycerol. Generation of a peroxisome proliferator-activated receptor alpha agonist. *J. Biol. Chem.* **277:** 23278–23286.
13. Lo Verme, J., J. Fu, G. Astarita, G. La Rana, R. Russo, A. Calignano, and D. Piomelli. 2005. The nuclear receptor peroxisome proliferator-activated receptor-alpha mediates the anti-inflammatory actions of palmitoylethanolamide. *Mol. Pharmacol.* **67:** 15–19.
14. Romano, M. R., and M. D. Lograno. 2012. Involvement of the peroxisome proliferator-activated receptor (PPAR) alpha in vascular response of endocannabinoids in the bovine ophthalmic artery. *Eur. J. Pharmacol.* **683:** 197–203.
15. Sun, Y., S. P. H. Alexander, M. J. Garle, C. L. Gibson, K. Hewitt, S. P. Murphy, D. A. Kendall, and A. J. Bennett. 2007. Cannabinoid activation of PPAR alpha; a novel neuroprotective mechanism. *Br. J. Pharmacol.* **152:** 734–743.
16. Sun, Y., S. P. H. Alexander, D. A. Kendall, and A. J. Bennett. 2006. Cannabinoids and PPARalpha signalling. *Biochem. Soc. Trans.* **34:** 1095–1097.
17. Jhaveri, M. D., D. Richardson, I. Robinson, M. J. Garle, A. Patel, Y. Sun, D. R. Sagar, A. J. Bennett, S. P. H. Alexander, D. A. Kendall, et al. 2008. Inhibition of fatty acid amide hydrolase and cyclooxygenase-2 increases levels of endocannabinoid related molecules and produces analgesia via peroxisome proliferator-activated receptor-alpha in a model of inflammatory pain. *Neuropharmacology.* **55:** 85–93.
18. Justinova, Z., L. V. Panlilio, G. Moreno-Sanz, G. H. Redhi, A. Auber, M. E. Secci, P. Mascia, T. Bandiera, A. Armirotti, R. Bertorelli, et al. 2015. Effects of fatty acid amide hydrolase (FAAH) inhibitors in non-human primate models of nicotine reward and relapse. *Neuropsychopharmacology.* **40:** 2185–2197.
19. Luchicchi, A., S. Lecca, S. Carta, G. Pillolla, A. L. Muntoni, S. Yasar, S. R. Goldberg, and M. Pistis. 2010. Effects of fatty acid amide hydrolase inhibition on neuronal responses to nicotine, cocaine and morphine in the nucleus accumbens shell and ventral tegmental area: involvement of PPAR-alpha nuclear receptors. *Addict. Biol.* **15:** 277–288.
20. Mazzola, C., J. Medalie, M. Scherma, L. V. Panlilio, M. Solinas, G. Tanda, F. Drago, J. L. Cadet, S. R. Goldberg, and S. Yasar. 2009. Fatty acid amide hydrolase (FAAH) inhibition enhances memory acquisition through activation of PPAR-alpha nuclear receptors. *Learn. Mem.* **16:** 332–337.
21. Sagar, D. R., D. A. Kendall, and V. Chapman. 2008. Inhibition of fatty acid amide hydrolase produces PPAR-alpha-mediated analgesia in a rat model of inflammatory pain. *Br. J. Pharmacol.* **155:** 1297–1306.
22. Izzo, A. A., and M. Camilleri. 2009. Cannabinoids in intestinal inflammation and cancer. *Pharmacol. Res.* **60:** 117–125.
23. Kozono, S., T. Matsuyama, K. K. Biwasa, K. Kawahara, Y. Nakajima, T. Yoshimoto, Y. Yonamine, H. Kadomatsu, S. Tancharoen, T. Hashiguchi, et al. 2010. Involvement of the endocannabinoid system in periodontal healing. *Biochem. Biophys. Res. Commun.* **394:** 928–933.
24. Whyte, L. S., E. Ryberg, N. A. Sims, S. A. Ridge, K. Mackie, P. J. Greasley, R. A. Ross, and M. J. Rogers. 2009. The putative cannabinoid receptor GPR55 affects osteoclast function in vitro and bone mass *in vivo*. *Proc. Natl. Acad. Sci. USA.* **106:** 16511–16516.
25. Yu, T. S., Z. H. Cheng, L. Q. Li, R. Zhao, Y. Y. Fan, Y. Du, W. X. Ma, and D. W. Guan. 2010. The cannabinoid receptor type 2 is time-dependently expressed during skeletal muscle wound healing in rats. *Int. J. Legal Med.* **124:** 397–404.
26. Idris, A. I. 2010. Cannabinoid receptors as target for treatment of osteoporosis: a tale of two therapies. *Curr. Neuropharmacol.* **8:** 243–253.
27. Ofek, O., M. Karsak, N. Leclerc, M. Fogel, B. Frenkel, K. Wright, J. Tam, M. Attar-Namdar, V. Kram, E. Shohami, et al. 2006. Peripheral cannabinoid receptor, CB_2, regulates bone mass. *Proc. Natl. Acad. Sci. USA.* **103:** 696–701.
28. Tam, J., V. Trembovler, V. Di Marzo, S. Petrosino, G. Leo, A. Alexandrovich, E. Regev, N. Casap, A. Shteyer, C. Ledent, et al. 2008. The cannabinoid CB_1 receptor regulates bone formation by modulating adrenergic signaling. *FASEB J.* **22:** 285–294.
29. Lastres-Becker, I., and J. Fernandez-Ruiz. 2006. An overview of Parkinson's disease and the cannabinoid system and possible benefits of cannabinoid-based treatments. *Curr. Med. Chem.* **13:** 3705–3718.
30. Zhang, X., Y. Maor, J. F. Wang, G. Kunos, and J. E. Groopman. 2010. Endocannabinoid-like N-arachidonoyl serine is a novel pro-angiogenic mediator. *Br. J. Pharmacol.* **160:** 1583–1594.
31. Yang, H., Z. Wang, J. E. Capo-Aponte, F. Zhang, Z. Pan, and P. S. Reinach. 2010. Epidermal growth factor receptor transactivation by the cannabinoid receptor (CB_1) and transient receptor potential vanilloid 1 (TRPV1) induces differential responses in corneal epithelial cells. *Exp. Eye Res.* **91:** 462–471.
32. Wright, K., N. Rooney, M. Feeney, J. Tate, D. Robertson, M. Welham, and S. Ward. 2005. Differential expression of cannabinoid receptors in the human colon: cannabinoids promote epithelial wound healing. *Gastroenterology.* **129:** 437–453.
33. Schmuhl, E., R. Ramer, A. Salamon, K. Peters, and B. Hinz. 2014. Increase of mesenchymal stem cell migration by cannabidiol via activation of p42/44 MAPK. *Biochem. Pharmacol.* **87:** 489–501.

34. Huang, J., Z. P. Zhang, J. A. Guo, A. G. Ni, A. Deb, L. N. Zhang, M. Mirotsou, R. E. Pratt, and V. J. Dzau. 2010. Genetic modification of viability, migration, engraftment, and capillary density in the injured myocardium. *Circ. Res.* **106:** 1753–1762.
35. Qin, Y., J. Guan, and C. Zhang. 2014. Mesenchymal stem cells: mechanisms and role in bone regeneration. *Postgrad. Med. J.* **90:** 643–647.
36. Walker, J. L., N. Zhai, L. P. Zhang, B. M. Bleaken, I. Wolff, J. Gerhart, M. George-Weinstein, and A. S. Menko. 2010. Unique precursors for the mesenchymal cells involved in injury response and fibrosis. *Proc. Natl. Acad. Sci. USA.* **107:** 13730–13735.
37. Shoji, T., M. Ii, Y. Mifune, T. Matsumoto, A. Kawamoto, S. M. Kwon, T. Kuroda, R. Kuroda, M. Kurosaka, and T. Asahara. 2010. Local transplantation of human multipotent adipose-derived stem cells accelerates fracture healing via enhanced osteogenesis and angiogenesis. *Lab. Invest.* **90:** 637–649.
38. Yao, W., M. Guan, J. J. Jia, W. W. Dai, Y. A. E. Lay, S. Amugongo, R. W. Liu, D. Olivos, M. Saunders, K. S. Lam, et al. 2013. Reversing bone loss by directing mesenchymal stem cells to the bone. *Stem Cells.* **31:** 2003–2014.
39. Aguado, T., K. Monory, J. Palazuelos, N. Stella, B. Cravatt, B. Lutz, G. Marsicano, Z. Kokaia, M. Guzman, and I. Galve-Roperh. 2005. The endocannabinoid system drives neural progenitor proliferation. *FASEB J.* **19:** 1704–1706.
40. Goncalves, M. B., P. Suetterlin, P. Yip, F. Molina-Holgado, D. J. Walker, M. J. Oudin, M. P. Zentar, S. Pollard, R. J. Yanez-Munoz, G. Williams, et al. 2008. A diacylglycerol lipase-CB_2 cannabinoid pathway regulates adult subventricular zone neurogenesis in an age-dependent manner. *Mol. Cell. Neurosci.* **38:** 526–536.
41. Rashid, M. A., M. Katakura, G. Kharebava, K. Kevala, and H. Y. Kim. 2013. N-Docosahexaenoylethanolamine is a potent neurogenic factor for neural stem cell differentiation. *J. Neurochem.* **125:** 869–884.
42. Xie, H., X. Sun, Y. Piao, A. G. Jegga, S. Handwerger, M. S. Ko, and S. K. Dey. 2012. Silencing or amplification of endocannabinoid signaling in blastocysts via CB_1 compromises trophoblast cell migration. *J. Biol. Chem.* **287:** 32288–32297.
43. Bab, I., R. Smoum, H. Bradshaw, and R. Mechoulam. 2011. Skeletal lipidomics: regulation of bone metabolism by fatty acid amid hydrolase family. *Br. J. Pharmacol.* **163:** 1441–1446.
44. Sophocleous, A., E. Landao-Bassonga, R. J. Van't Hof, A. I. Idris, and S. H. Ralston. 2011. The type 2 cannabinoid receptor regulates bone mass and ovariectomy-induced bone loss by affecting osteoblast differentiation and bone formation. *Endocrinology.* **152:** 2141–2149.
45. Gao, H., W. Priebe, J. Glod, and D. Banerjee. 2009. Activation of signal transducers and activators of transcription 3 and focal adhesion kinase by stromal cell-derived factor 1 is required for migration of human mesenchymal stem cells in response to tumor cell-conditioned medium. *Stem Cells.* **27:** 857–865.
46. Yun, D. H., H. Y. Song, M. J. Lee, M. R. Kim, M. Y. Kim, J. S. Lee, and J. H. Kim. 2009. Thromboxane A_2 modulates migration, proliferation, and differentiation of adipose tissue-derived mesenchymal stem cells. *Exp. Mol. Med.* **41:** 17–24.
47. Ahn, K., D. S. Johnson, L. R. Fitzgerald, M. Liimatta, A. Arendse, T. Stevenson, E. T. Lund, R. A. Nugent, T. K. Nomanbhoy, J. P. Alexander, et al. 2007. Novel mechanistic class of fatty acid amide hydrolase inhibitors with remarkable selectivity. *Biochemistry.* **46:** 13019–13030.
48. Alexander, J. P., and B. F. Cravatt. 2005. Mechanism of carbamate inactivation of FAAH: implications for the design of covalent inhibitors and in vivo functional probes for enzymes. *Chem. Biol.* **12:** 1179–1187.
49. Mor, M., S. Rivara, A. Lodola, P. V. Plazzi, G. Tarzia, A. Duranti, A. Tontini, G. Piersanti, S. Kathuria, and D. Piomelli. 2004. Cyclohexylcarbamic acid 3′- or 4′-substituted biphenyl-3-yl esters as fatty acid amide hydrolase inhibitors: synthesis, quantitative structure-activity relationships, and molecular modeling studies. *J. Med. Chem.* **47:** 4998–5008.
50. Bisogno, T., D. Melck, L. De Petrocellis, M. Bobrov, N. M. Gretskaya, V. V. Bezuglov, N. Sitachitta, W. H. Gerwick, and V. Di Marzo. 1998. Arachidonoylserotonin and other novel inhibitors of fatty acid amide hydrolase. *Biochem. Biophys. Res. Commun.* **248:** 515–522.
51. Ivanov, I., P. Borchert, and B. Hinz. 2015. A simple method for simultaneous determination of N-arachidonoylethanolamine, N-oleoylethanolamine, N-palmitoylethanolamine and 2-arachidonoylglycerol in human cells. *Anal. Bioanal. Chem.* **407:** 1781–1787.
52. Ramer, R., and B. Hinz. 2008. Inhibition of cancer cell invasion by cannabinoids via increased expression of tissue inhibitor of matrix metalloproteinases-1. *J. Natl. Cancer Inst.* **100:** 59–69.
53. Xu, X., M. Otsuki, S. Sumitani, H. Saito, H. Kouhara, and S. Kasayama. 2002. RU486 antagonizes the inhibitory effect of peroxisome proliferator-activated receptor alpha on interleukin-6 production in vascular endothelial cells. *J. Steroid Biochem. Mol. Biol.* **81:** 141–146.
54. Song, Z. H., and M. Zhong. 2000. CB_1 cannabinoid receptor-mediated cell migration. *J. Pharmacol. Exp. Ther.* **294:** 204–209.
55. Burns, K. A., and J. P. Vanden Heuvel. 2007. Modulation of PPAR activity via phosphorylation. *Biochim. Biophys. Acta.* **1771:** 952–960.
56. Shalev, A., C. A. Siegrist-Kaiser, P. M. Yen, W. Wahli, A. G. Burger, W. W. Chin, and C. A. Meier. 1996. The peroxisome proliferator-activated receptor alpha is a phosphoprotein: regulation by insulin. *Endocrinology.* **137:** 4499–4502.
57. Juge-Aubry, C. E., E. Hammar, C. Siegrist-Kaiser, A. Pernin, A. Takeshita, W. W. Chin, A. G. Burger, and C. A. Meier. 1999. Regulation of the transcriptional activity of the peroxisome proliferator-activated receptor alpha by phosphorylation of a ligand-independent trans-activating domain. *J. Biol. Chem.* **274:** 10505–10510.
58. Rotman, N., and W. Wahli. 2010. PPAR modulation of kinase-linked receptor signaling in physiology and disease. *Physiology (Bethesda).* **25:** 176–185.
59. Werner, C. M., S. H. Schirmer, C. Gensch, V. Pavlickova, J. Poss, M. B. Wright, M. Bohm, and U. Laufs. 2014. The dual PPARα/γ agonist aleglitazar increases the number and function of endothelial progenitor cells: implications for vascular function and atherogenesis. *Br. J. Pharmacol.* **171:** 2685–2703.
60. Hornung, D., L. L. Waite, E. A. Ricke, F. Bentzien, D. Wallwiener, and R. N. Taylor. 2001. Nuclear peroxisome proliferator-activated receptors alpha and gamma have opposing effects on monocyte chemotaxis in endometriosis. *J. Clin. Endocrinol. Metab.* **86:** 3108–3114.
61. Stephen, J., C. Delvecchio, N. Spitale, A. Giesler, K. Radford, P. Bilan, P. G. Cox, J. P. Capone, and P. Nair. 2013. PPAR ligands decrease human airway smooth muscle cell migration and extracellular matrix synthesis. *Eur. Respir. J.* **41:** 425–432.
62. Goetze, S., F. Eilers, A. Bungenstock, U. Kintscher, P. Stawowy, F. Blaschke, K. Graf, R. E. Law, E. Fleck, and M. Gräfe. 2002. PPAR activators inhibit endothelial cell migration by targeting Akt. *Biochem. Biophys. Res. Commun.* **293:** 1431–1437.